ENVIRONMENTAL RESEARCH
LETTERS

LETTER • OPEN ACCESS

Constraining the projections of tropical extreme precipitation with radiation–precipitation relationship

To cite this article: Yuanyuan Huang *et al* 2026 *Environ. Res. Lett.* **21** 044003

IOP Publishing Environ. Res. Lett. 21 (2026) 044003 https://doi.org/10.1088/1748-9326/ae4117

ENVIRONMENTAL RESEARCH
LETTERS

OPEN ACCESS

RECEIVED
2 December 2025

REVISED
29 January 2026

ACCEPTED FOR PUBLICATION
3 February 2026

PUBLISHED
19 February 2026

LETTER

Constraining the projections of tropical extreme precipitation with radiation–precipitation relationship

Yuanyuan Huang[1], **Zhijian Yang**[2] **and Xiaoming Shi**[1,3,*]

[1] Division of Environment and Sustainability, The Hong Kong University of Science and Technology, Hong Kong Special Administrative Region of China, People's Republic of China
[2] Department of Mechanical Engineering, National University of Singapore, Singapore, Singapore
[3] Center for Ocean Research in Hong Kong and Macau, Hong Kong, People's Republic of China
[*] Author to whom any correspondence should be addressed.

E-mail: shixm@ust.hk

Keywords: cloud-radiative effect, extreme precipitation, emergent constraint

Supplementary material for this article is available online

Abstract

Over the tropics, a robust statistical relationship between outgoing longwave radiation (R) and precipitation (P) is observed, linked to the cloud-radiative effect (CRE). To quantify this R–P relation, we define the CRE parameter, which exhibits significant disparities across global climate models (GCMs), with most overestimating it relative to the observation. Given the strong correlation between the CRE parameter and both historical and future extreme precipitation, an emergent constraint on the hydrological cycle projection is constructed. It lowers the fractional increase in the 99.9th percentile of tropical precipitation by the end of the 21st century from 29% to 24% under the high-emission warming scenario, with a 58% reduction in uncertainty. Overall, GCMs tend to underestimate the intensity of tropical extreme precipitation while overestimating its fractional increase. These findings provide valuable insights for model evaluation, improvement, and climate adaptation strategies.

1. Introduction

The hydrological cycle is undergoing significant changes due to global warming, with profound implications on both global and regional scales [1–3]. Among these, intensifying extreme rainfall events pose a growing threat [4, 5], causing severe damage to infrastructure and loss of life [6]. Despite widespread recognition of these impacts, projecting future changes in mean and extreme precipitation remains highly uncertain across global climate models (GCMs) [7, 8], particularly over the tropics [2, 9]. For instance, under the high-emission warming scenario, the projected fractional change in the extreme precipitation by the end of the 21st century relative to the current climate state varies widely across GCMs, ranging from 17.6% to 44.9% [10]. These uncertainties stem from multiple factors, including differences in physical parameterizations and internal variabilities [2, 7]. Consequently, more reliable and accurate projections are vital for stakeholders to assess risks and implement effective adaptation strategies.

The emergent constraint is a popular method to constrain future projections based on known observations, which has been increasingly applied to various climatic quantities or their relative changes (i.e. fractional change and sensitivity to global warming), such as precipitation [8, 11–13], surface temperature [14–16], snow albedo feedback [17], and jet shift [18]. For the extreme precipitation-related constraints, most studies rely on temperature [8], the extreme precipitation variability [11, 19], or other hydrological sensitivity [20] as key predictors. For example, one study [11] revealed the significant emergent relationship between extreme precipitation sensitivities for interannual variability and climate change, although his constraints did not comprehensively address the uncertainty issues. The other study [19] used present-day precipitation variability to constrain the quantity associated with the occurrence probability of extreme events, though the reliability of this constraint varied across precipitation events. Recently, the radiative effect has been introduced as a potential constraint on precipitation-related

projections [13, 21], highlighting the strong connection between the radiative effect and precipitation.

In the tropical atmosphere, radiation changes and precipitation generation are likely to have a close connection, especially within a specific period without greenhouse gas-induced climate change. Previous studies have noticed the radiation–precipitation relation (hereafter referred to as the *R–P* relation). It can be expressed in a simplified form when encapsulating the cloud-radiative effect (CRE) to solve the analytical models of tropical waves or circulations [22–24]. Other studies also discussed the *R–P* relation from different perspectives and for different purposes, such as different temporal scales, datasets (observational or numerical), and applications [25–28]. For instance, the *R–P* relation was expressed as a 'greenhouse enhancement factor' in a Madden–Julian oscillation (MJO) study [25], where the correct representation of the *R–P* relation in GCMs was suggested to be crucial in the MJO simulations. Besides, the observed *R–P* relation could also be used to classify the local departures from the tropics-wide radiative-convective equilibrium [26]. Despite those efforts, no unified expression for the *R–P* relation currently exists, and the past observational data are limited. These make the *R–P* relation still worth further investigation. Considering the demonstrated importance and availability of the *R–P* relation in the tropics, the *R–P* relation seems to hold great potential for constraining tropical precipitation projections.

Given the aforementioned scientific significance and existing research gaps, this study examines the *R–P* relation over the tropics using the observational data and simulation data from Coupled Model Intercomparison Project Phase 6 (CMIP6). We also apply this relationship to constrain the projections of current and future tropical extreme precipitation intensity and their fractional change relative to the current climate. This study extends beyond theoretical exploration, offering practical insights into improving future climate predictions and informing strategies for climate adaptation.

2. Data and methods

The daily observational precipitation data are sourced from the NASA Integrated Multi-satellitE Retrievals for Global Precipitation Measurement mission version 07. Additionally, daily blended outgoing longwave radiation (OLR) data from the National Oceanic and Atmospheric Administration Climate Prediction Center are used in this study. Further details on other observational datasets used for comparison can be found in text S1. For model-based calculations, we selected historical data along with two warming scenarios (SSP2-4.5 and SSP5-8.5) from 21 CMIP6 models (table S1). All data are regridded to a common $2.5° \times 2.5°$ grid using the areal conservative method. The period from 2001 to 2014 (14 years) is selected for the calculations of observation and historical data to represent the current climate state. The period of 2081–2100 (20 years) is selected as the future state. All the calculations are considered within the tropics (20°S–20°N). Additional details on the datasets can be found in text S1.

The emergent constraint method adopted in this study is according to [18], which comprehensively considers the uncertainty issues, showing more convincing constraint results compared to some previous studies. Based on the ordinary least squares regression, the distribution of the projected quantity y is estimated by the predictor x. The uncertainties of y incorporate (i) the uncertainty on the linear relationship (i.e. emergent constraint itself), (ii) the uncertainties on the internal variability of x and y, and (iii) the uncertainty associated with inter-model differences, aside from those explained by emergent constraint. Besides, we also consider the regression uncertainty of x (x is a ratio in this study). More details of the emergent constraint method are described in text S3.

3. Radiation–precipitation relationship

To address the *R–P* relation over the tropics (20°S–20°N), we first show the joint probability distribution function (PDF) of OLR and precipitation anomalies in the current climate state using the observational data (figure 1(a)). The removed linear trend and seasonal cycle result in a stable statistical estimation without considering the seasonal cycle and climate change within a selected period. Thus, the OLR changes in a climate state mainly come from the CRE while neglecting the influences of anthropogenic warming.

Overall, the observed tropical *R–P* relation exhibits its non-linearity, showing an averaged curve with a reverse-'S' shape. The OLR decreases with increasing precipitation, indicating that generating convection is associated with the absorbed longwave (LW) radiation in the atmosphere due to clouds, leading to atmospheric radiative heating. Note that in the regime with strong precipitation anomalies, the OLR decreases more slowly than in the other regimes. This nonlinear relationship is primarily due to the principle of radiative transfer in the atmosphere. As precipitation intensifies, the amount of cloud droplets and ice particles increases in convective storms, which determines the optical depth of atmospheric layers and, in turn, determines the fraction of radiative flux absorbed by a layer. Thus, as precipitation intensifies, the amount of absorbed radiative flux saturates.

Figure 1(b) shows the multi-model mean (MMM) joint PDF of tropical OLR and precipitation anomalies from CMIP6 historical simulations. A similar *R–P* relation with a reverse-'S' shape is well simulated. However, the varying fidelity in reproducing the tropical *R–P* relation across GCMs is evidenced

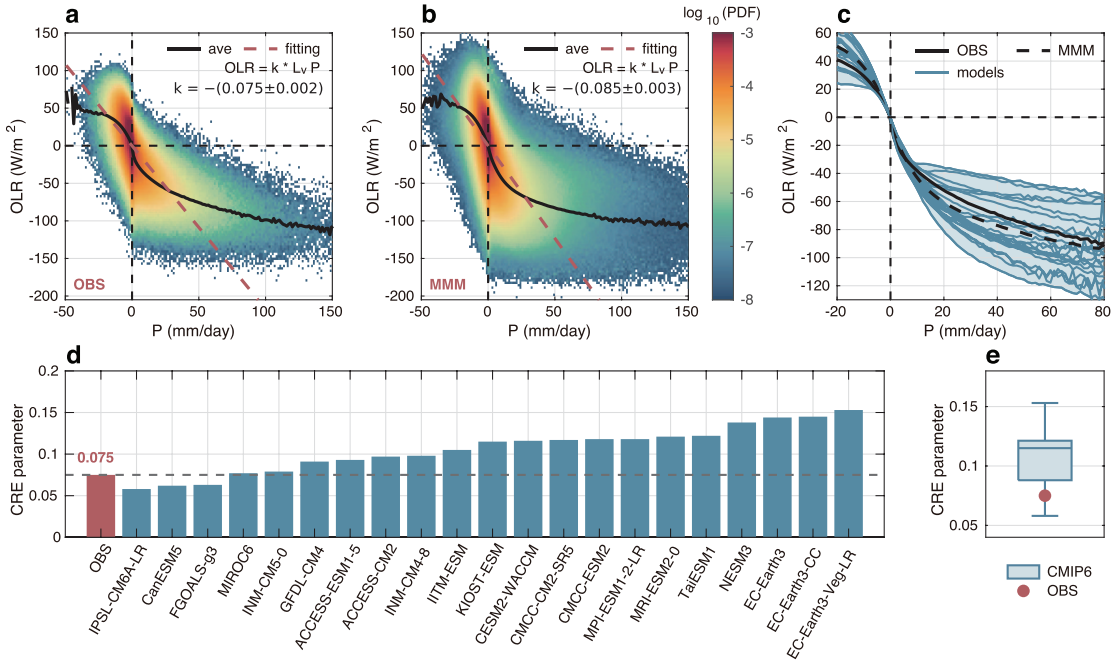

Figure 1. (a) Joint PDF of observed tropical (20°S–20°N) OLR anomaly and precipitation anomaly at individual grid cells during 2001–2014. The linear trend and seasonal cycle are removed from the OLR and precipitation data. The black curve is calculated as the averaged OLR anomaly at each precipitation anomaly. The dashed red line is the linear fit of precipitation anomaly and OLR anomaly through ordinary least squares regression, weighted by the joint PDF. (b) Same as in (a), but for the multi-model mean (MMM) the joint PDF of 21 CMIP6 models. (c) Averaged curves, as the curves in (a) and (b), of the observation (black solid curve), the individual CMIP6 models (blue curves), and the MMM of CMIP6 models (black dashed curve). (d) The observed CRE parameter (red bar) and the CRE parameters across CMIP6 models (blue bars). (e) The boxplot of the CRE parameters across the CMIP6 models. The horizontal line in the box indicates the median. The top and bottom edges of a box indicate the 25th and 75th percentiles, respectively. The extending whiskers indicate the maximum and minimum. The red dot represents the observed CRE parameter.

by varying mean slopes of the averaged curves and upper limits of OLR anomaly (figure S1). Figure 1(c) further compares the expectations of OLR anomaly as a function of precipitation anomaly for observation, individual CMIP6 models, and MMM. Around the median, the MMM exhibits a steeper slope of the averaged curve compared to the observation, indicating that most GCMs are inclined to trap more radiative flux by clouds and lead to stronger radiative heating relative to the observation when generating the same amount of precipitation. In other words, most GCMs generate less precipitation in response to similar radiative forcing, meaning that their convective clusters have a lower precipitation efficiency associated with the CRE.

Despite the non-linearity of the *R–P* relation, the high probability density concentrates around the median precipitation to strong precipitation (0–40 mm d^{-1}), which should dominantly influence the slope of the regression line. Thus, a linear estimation is still a rational simplification to measure the *R–P* relation semi-quantitatively, aligning with previous studies that have similarly emphasized the estimated linear relationship [23, 25]. Our study defines a linear estimation for the *R–P* relation as the ratio of OLR and precipitation anomalies over the tropics obtained through linear regression, named the CRE parameter (denoted by γ in equations):

$$OLR' = -\gamma P', \tag{1}$$

where the prime ($'$) represents the anomaly of a quantity. The dimension sizes of OLR' and P' are $ntim \times nlat \times nlon$, where the *ntim*, *nlat*, and *nlon* are the dimension sizes of time, latitude, and longitude, respectively. Before applying the ordinary least squares regression, the precipitation data is scaled by the latent heat of evaporation L_v to convert the unit from mm d^{-1} to W m^{-2}; the OLR and precipitation data are removed the linear trend and seasonal cycle, since we expect the CRE parameter to be a stable statistic without considering the seasonal variation and the effect of climate change with a selected period. All the temporal and spatial points without any average or smoothing are used in the calculation. A higher CRE parameter suggests that for the same latent heating, more cloud radiative heating is produced; alternatively, for the same cloud radiative heating, less latent heating (precipitation) is generated (figure 2). It indicates a relatively low precipitation efficiency associated with CRE in convective storms. Similarly, a lower CRE parameter indicates a relatively high precipitation efficiency associated with CRE.

Figures 1(d) and (e) compare the present-day CRE parameters across GCMs with the observed CRE parameter (0.075). The results show significant variance in model performance, with most GCMs overestimating the CRE parameter. If comparing to other sets of observation data, the CRE parameters across GCMs still show a quantitative consistency—overestimating relative to the observations (table S3).

Despite its simplicity, the CRE parameter remains a valuable metric that measures different radiation-convection interactions in both real world and GCMs. The variation in the CRE parameters across different GCMs is likely attributed to the different representations of cumulus convection, cloud microphysics, turbulence, radiation, and their interaction in the physical parameterization schemes, which affect precipitation efficiency and organization of convective storms in GCMs [29, 30]. For example, a previous study suggested that the shallow-to-deep transition and the vertical wind shear in parameterizations are crucial for simulating mesoscale organization of convective systems, and, thereby, the *R–P* relation [25]. Another study suggested that conventional microphysics schemes have inconsistent formulations for ice phase processes, and innovative scheme design is needed to improve GCM microphysics [31].

4. Constraining the extreme precipitation projection

Extreme precipitation in this study is defined using a specified percentile of temporally and spatially aggregated daily precipitation. All data points over the tropics (20°S–20°N) during 2001–2014 are used as analysis samples, representing the stable statistical characteristics of tropical extreme precipitation under a given climate state. The 99.9th percentile of precipitation is referred to as the extreme precipitation intensity $P_{e,99.9}$, which is considered for main calculations. The scatter plots in figure 3 show the inter-model correlations between the CRE parameters and historical extreme precipitation as well as the future extreme precipitation by the end of the 21st century over the tropics. Strong negative correlations are evident in historical data and two warming scenarios. The correlation coefficient reaches −0.94 for the historical extreme precipitation and −0.85 (−0.76) under the SSP2-4.5 (SSP5-8.5) warming scenario. The correlations of other percentiles (98th, 99th, 99.5th, 99.8th, and 99.95th) of precipitation and their correlation uncertainties estimated via bootstrapping are shown in figure S2. The robust negative correlations highlight an emergent relationship, suggesting that the CRE parameter can serve as a predictor to constrain the tropical extreme precipitation and may help to reduce the inter-model uncertainties. Note that the correlations for the 98th percentile of precipitation ($P_{e,98}$) are relatively weak (figure S2), thus, we exclude this case from subsequent emergent constraint calculations.

Regardless of the evolution of the CRE parameter under climate change, the present-day CRE parameter calculated by historical simulations could be a measure of the background state for convective storm generation in a given GCM. When the CRE parameter is higher, although generating extreme precipitation requires stronger cloud-radiative heating, it is constrained by the clouds' limited capacity of radiation absorption, thereby preventing extreme event generation. Conversely, a lower CRE parameter signifies more efficient convection formation, facilitating extreme precipitation generation with reduced reliance on extreme cloud radiative heating, thereby increasing the likelihood of extreme event occurrence. Therefore, the present-day CRE parameters can serve as an effective factor for constraining the future extreme precipitation projections over the tropics, with statistical (high correlations) and physical soundness. This constraint idea does not require knowing the values of the future CRE parameter, thereby avoiding the estimation bias associated with the future CRE values.

Figure 3(a) illustrates the uncertainty on the present-day CRE parameter, including the regression uncertainty of the CRE parameter and the internal variability estimated by the large ensemble members in CMIP6 (text S3). The variance of the CRE parameter ($\sigma_{xtot} = 0.0002$) is quite small. It is reasonable since the CRE parameter is a relatively stable statistical quantity due to the regression of a large sample and does not vary much between the different simulation realizations. Thus, the uncertainty of the CRE parameter does not mainly contribute to the total uncertainty of the future projections.

Applying the emergent constraint, the total uncertainties for the projected historical and future $P_{e,99.9}$ are shown by the PDF in figures 3(c), (e) and (g). These calculations encompass the uncertainty on the internal variability and regression of present-day CRE parameter (figure 3(a)), the uncertainty on emergent constraint itself (gray areas in figures 3(b), (d) and (f), the uncertainty on the internal variability of historical and future $P_{e,99.9}$, and the uncertainty associated with the inter-model differences which is not explained by the emergent constraint (the latter two not shown). For historical $P_{e,99.9}$, the constrained PDF is centered at 81.92 mm d^{-1}, with a 5%–95% confidence interval (CI) of 73.04–90.32 mm d^{-1}. Compared to the MMM $P_{e,99.9}$ before constraint (66.05 mm d^{-1}), the constrained value is closer to the observation (87.84 mm d^{-1}). Under the SSP2-4.5 scenario, the constrained projection of future $P_{e,99.9}$ reaches 92.74 mm d^{-1}, with a 5%–95% CI of 76.18–109.32 mm d^{-1}. For the SSP5-8.5 scenario, the constrained future $P_{e,99.9}$ reaches 101.36 mm d^{-1}, with a 5%–95% CI of 79.22–123.49 mm d^{-1}.

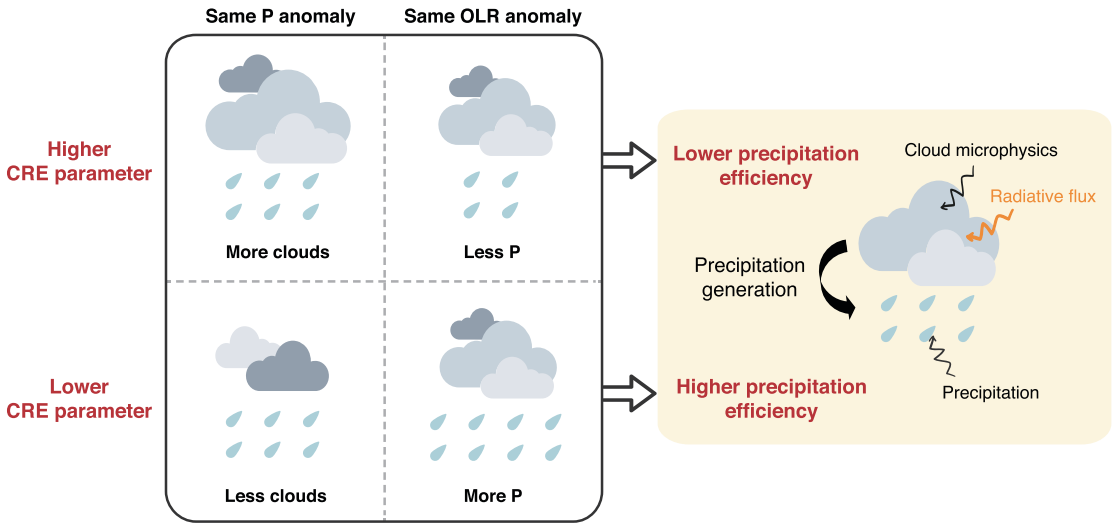

Figure 2. Schematic diagram of the physical meaning of the CRE parameter. On the left, it illustrates four scenarios. The first column compares the cloud amounts under different CRE parameters when the precipitation (P) anomaly is the same. The second column compares the precipitation amounts under different CRE parameters when the OLR anomaly is the same (approximately equivalent to the same cloud amount or the same cloud radiative heating). On the right, the precipitation generation induced by the interaction between cloud microphysics and radiative flux is depicted. This process reflects the precipitation efficiency associated with CRE.

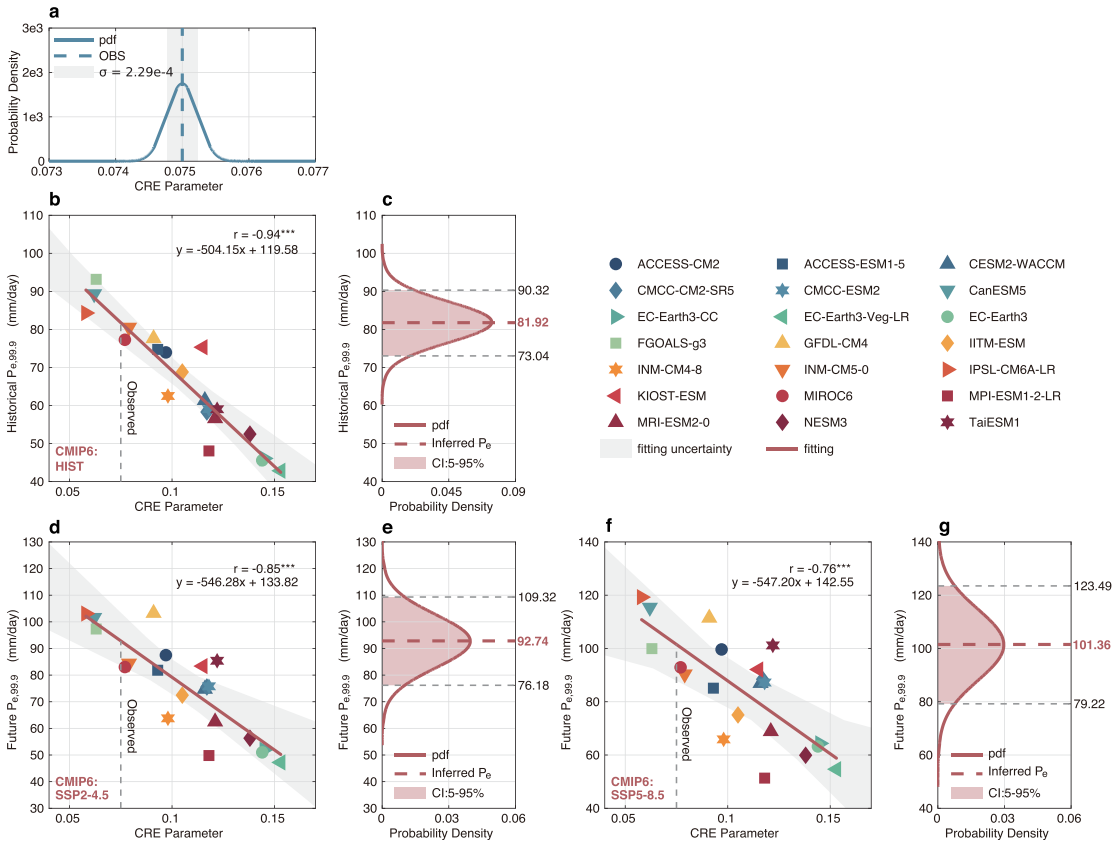

Figure 3. (a) The probability distribution of the possible values of the present-day CRE parameter (blue solid line), representing the uncertainty of the CRE parameter. The observed value is at the center of the PDF (blue dashed line). The gray area represents the standard deviation range ($\pm\sigma_{xtot} = \pm\sqrt{\sigma_x^2 + \sigma_{reg}^2}$) (text S3). (b) The scatter of present-day CRE parameters and the 99.9th percentile of precipitation ($P_{e,99.9}$) using historical data. The red line represents the ordinary least squares regression. The gray area represents the fitting uncertainty, which is filled within the envelope of 1000 regression lines relative to 1000 resampled regression coefficients. The gray dashed line indicates the value of the observed CRE parameter. (c) The probability distribution of the possible historical $P_{e,99.9}$ after constraint (red solid line), representing the uncertainty of historical $P_{e,99.9}$ projection. The mean value is shown by the red dashed line. The 5%–95% confidence intervals are shown in the light red area between the gray dashed lines. (d) and (f) The same as in (b), but for the future $P_{e,99.9}$ under the SSP2-4.5 scenario and SSP5-8.5 scenario, respectively. (e) and (g) The same as in (c), but for the future $P_{e,99.9}$ under the SSP2-4.5 scenario and SSP5-8.5 scenario, respectively. All the calculations are considered within the tropics (20°S–20°N).

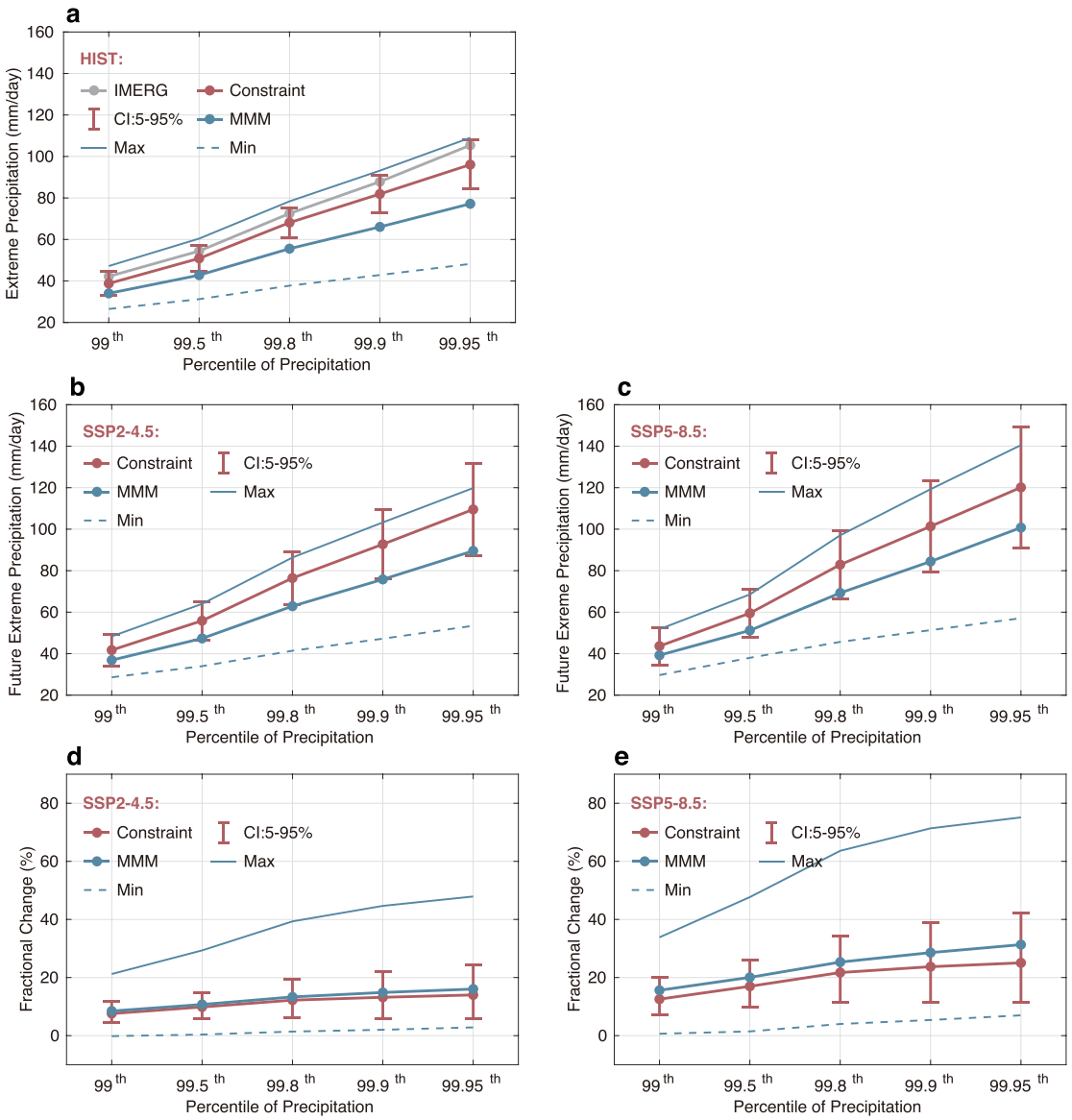

Figure 4. (a) The CMIP6 projections and the emergent constraint results of historical tropical extreme precipitation at different percentiles. The gray line represents the observational present-day extreme precipitation. The MMMs of historical extreme precipitation are shown in the blue line with dots. The other two blue lines show the model maxima and minima. The constrained historical extreme precipitation is shown in the red line, with red error bars denoting the 5%–95% confidence intervals. (b), (c) The same as in (a), but for the future extreme precipitation under the SSP2-4.5 scenario and the SSP5-8.5 scenario, respectively. (c), (d) The same as in (a), but for the fractional change of extreme precipitation $\Delta P_e/P_e$ under the SSP2-4.5 scenario and the SSP5-8.5 scenario, respectively.

Further comparisons between the CMIP6 projections and the constraint results across various percentiles of precipitation are shown in figures 4(a)–(c). In historical simulations and two warming scenarios, the GCMs in CMIP6, on average, underestimate extreme precipitation. After our emergent constraint, the future extreme precipitation increases to higher intensities and the uncertainty ranges are significantly reduced, as evident in the comparison between the 5%–95% CIs of constraint results (red error bars) and the inter-model scatters (thin blue lines) in figures 4(a)–(c). For details, the uncertainty of historical $P_{e,99.9}$ is reduced by 64.71%, and the uncertainty of $P_{e,99.9}$ under the SSP2-4.5 scenario (SSP5-8.5 scenario) is reduced by 40.87% (34.84%), highlighting that our constraint method is effective. The imperfect model test with the assessment of root mean square error, correlation, and coverage ratio also demonstrates the validity of our constraint method (figure S3).

Because the CRE parameter is a quantity used to characterize a climate state, it cannot be directly used to constrain a variable that includes an increment in the traditional way. This is also demonstrated by the low inter-model correlations between the present-day CRE parameter and fractional change of extreme precipitation by the end of this century relative to the historical period ($\Delta P_e/P_e = (P_{e,future} - P_{e,present})/P_{e,present} \times 100\%$) over the tropics (table S6). Therefore, we calculate

the constraint of fractional change $\Delta P_e/P_e$ using the constrained results of historical and future extreme precipitation rather than applying full emergent constraint processes, which is referred to as an 'indirect' constraint.

The constraint results for the fractional change are shown in figures 4(d) and (e). After applying the constraint, the fractional increases in tropical extreme precipitation by the end of the 21st century (relative to the present) become lower compared to the MMM before constraint, and the uncertainty ranges are significantly reduced under both warming scenarios. For example, considering the 99.9th percentile of precipitation: the $\Delta P_e/P_e$ lowers from 14.86% (MMM) to 13.02% under the SSP2-4.5 scenario, and its uncertainty is reduced by 62.23% from 2.02%–44.67% inter-model scatter to a constrained 5%–95% CI of 4.30%–20.40%; the $\Delta P_e/P_e$ lowers from 28.85% (MMM) to 23.75% under the SSP5-8.5 scenario and its uncertainty range narrows from 5.38%–71.37% to 8.46%–36.01%, with a reduction of 58.25%. Contrary to the underestimation of future tropical extreme precipitation intensity, most GCMs in CMIP6 overestimate the $\Delta P_e/P_e$. It indicates that those GCMs misrepresent how fast extreme precipitation intensity grows under global warming. Despite the future tropical extreme precipitation will intensify to a higher degree, it is reassuring that it will grow at a more moderate pace.

In addition, we also roughly estimate the climate sensitivities of tropical extreme precipitation to global warming without constraining the temperature. According to the CMIP6 simulations, the MMM global temperature rise by the end of the 21st century is 1.96 K and 3.73 K for the medium- and high-emission scenarios, respectively. It implies that, for example, the corresponding constrained sensitivities of tropical $P_{e,99.9}$ are approximately 6.73 $\%K^{-1}$ and 6.36 $\%K^{-1}$, lower than the unconstrained sensitivities 7.58$\%K^{-1}$ and 7.66$\%K^{-1}$. These rates are slightly lower than the 7$\%K^{-1}$ sensitivity suggested by the Clausius–Clapeyron scaling. The more moderate sensitivities are plausible, given that the dynamical processes, such as large-scale circulations, will exert negative influences under global warming, partially offsetting the thermodynamic effects [32].

5. Conclusion and discussion

We explored the statistical relationship between radiation and precipitation over the tropics at individual grid cells, where OLR decreases nonlinearly with increasing precipitation. To quantify this *R–P* relation, we introduce the 'CRE parameter', defined as the ratio of OLR and precipitation anomalies. The observed present-day CRE parameter is 0.075, while most GCMs overestimate it. The metric captures the critical role of CRE in modulating tropical convection. The different representations of *R–P* relations across GCMs are likely attributed to the differences in their physical parameterization schemes, such as cloud microphysical processes. Therefore, the *R–P* relation not only encapsulates the balance between radiative heating and latent heating anomalies in convective storms, offering valuable insights for better comprehending the cloud-radiation-convection feedback, but also serves as an effective measurement for model evaluation.

While our results focus on the *R–P* relation in tropical regions, whether this relationship can be extended to other regions remains unclear and requires further calculations and investigation. In particular, applications to higher latitudes may need to account for additional factors such as latitude-dependent area weighting and the influence of heterogeneous lower boundary conditions brought by the continents.

The projections of historical and future extreme precipitation, as well as their fractional change, exhibit significant uncertainties across GCMs. Due to the emergent relationship with high inter-model correlations between the present-day CRE parameter and extreme precipitation over the tropics, the *R–P* relation provides an alternative possibility to constrain the extreme precipitation projections. Under the medium-emission (high-emission) warming scenario, the constrained $P_{e,99.9}$ reaches 92.74 mm d^{-1} (101.36 mm d^{-1}), with uncertainty reduced by 40.87% (34.84%). The constrained future $P_{e,99.9}$ is larger than the unconstrained MMM. Its corresponding fractional increase by the end of the 21st century is lowered from the unconstrained value of 14.86% (28.85%) to 13.02% (23.75%) after applying the constraint, and the uncertainty is significantly reduced by 62.23% (58.25%). These constraint results highlight that the CMIP6 models underestimate the intensity of future tropical extreme precipitation while overestimating its fractional change. It is known that GCMs underestimate extreme precipitation intensity due to their coarse resolutions. Our emergent constraint yields more realistic projections for future periods, providing both theoretical insight and practical value. Despite the future tropical extreme precipitation will intensify to a higher degree, it is reassuring that it will grow at a more moderate pace, not as large as previous studies suggested.

Despite the limited length of the historical precipitation and OLR records available for calculating the observed CRE parameter over the tropics, our study still offers a novel perspective on understanding the CRE. The CRE parameter is introduced for the first time to constrain the precipitation-related quantities, demonstrating significant effectiveness. In addition to its novelty, the CRE parameter is a stable metric

with very small uncertainty (including both internal variability and regression uncertainty), which helps reduce the total uncertainty in emergent constraint. Our emergent constraint also complements previous studies, which primarily focus on atmospheric dynamics, interannual variability, and physical parameterizations in understanding the tropical extremes.

Note that the calculation of extreme precipitation in this study has limitations, as the temporal and spatial aggregation of precipitation data may artificially increase the effective sample size and influence extreme precipitation estimates due to non-independence among individual grids. Consequently, the spatial correlations and regional-scale characteristics of the *R–P* relation and extreme precipitation warrant further investigation. Previous studies have demonstrated the feasibility of constraining future projections at regional scales [8, 19, 20]. In this context, we present an additional, preliminary analysis of the spatial inter-model correlations between the CRE parameter and future extreme precipitation in figure S4. Statistically significant correlations are found over the warm pool region and the Intertropical Convergence Zone, suggesting that the emergent relationship is regionally dependent. Our future work will focus on the regional *R–P* relations (or their spatial distribution) and their potential to constrain future hydrological responses across the tropics and even higher latitudes, which could provide valuable insights for improving regional climate adaptation.

Data availability statement

The data that support the findings of this study are openly available at the following URL/DOI:. https://doi.org/10.5281/zenodo.14 964 799 [33]. The CMIP6 output is available at https://esgf-node.llnl.gov/projects/.The NASA IMERG version 07 daily precipitation data are available at https://gpm.nasa.gov/resources/documents/imerg-v07-release-notes. The NOAA/CPC daily blended OLR data are available at https://psl.noaa.gov/data/gridded/.

Acknowledgments

We thank the two anonymous reviewers for their constructive comments and suggestions, which helped improve the clarity and quality of this manuscript. We acknowledge the Paul O'Gorman, who kindly shared his views on this Project. The work described in this paper was substantially supported by a grant from the Research Grants Council (RGC) of the Hong Kong Special Administrative Region, China (Project Reference: AoE/P-601/23-N). X S was additionally supported by the Center for Ocean Research in Hong Kong and Macau (CORE), a joint research center between the Laoshan Laboratory and Technology and the Hong Kong University of Science and Technology (HKUST), and RGC Grant HKUST-16307323.

Author contributions

Yuanyuan Huang 0000-0003-4206-2632
Conceptualization (lead), Data curation (lead), Formal analysis (lead), Investigation (lead), Methodology (lead), Validation (lead), Visualization (lead), Writing – original draft (lead), Writing – review & editing (lead)

Zhijian Yang 0000-0002-8287-4267
Formal analysis (supporting), Methodology (equal), Software (equal), Visualization (supporting), Writing – review & editing (supporting)

Xiaoming Shi 0000-0002-5329-7851
Conceptualization (equal), Funding acquisition (lead), Investigation (supporting), Project administration (lead), Resources (lead), Supervision (lead), Writing – review & editing (equal)

References

[1] Allen M R and Ingram W J 2002 Constraints on future changes in climate and the hydrologic cycle *Nature* **419** 224–32
[2] O'Gorman P A and Schneider T 2009 The physical basis for increases in precipitation extremes in simulations of 21st-century climate change *Proc. Natl Acad. Sci.* **106** 14773–7
[3] Zhang W, Furtado K, Wu P, Zhou T, Chadwick R, Marzin C, Rostron J and Sexton D 2021 Increasing precipitation variability on daily-to-multiyear time scales in a warmer world *Sci. Adv.* **7** eabf8021
[4] Coumou D and Rahmstorf S 2012 A decade of weather extremes *Nat. Clim. Change* **2** 491–6
[5] Bao J, Stevens B, Kluft L and Muller C 2024 Intensification of daily tropical precipitation extremes from more organized convection *Sci. Adv.* **10** eadj6801
[6] Guo X, Cheng J, Yin C, Li Q, Chen R and Fang J 2023 The extraordinary Zhengzhou flood of 7/20, 2021: how extreme weather and human response compounding to the disaster *Cities* **134** 104168
[7] O'Gorman P A 2015 Precipitation extremes under climate change *Curr. Clim. Change Rep.* **1** 49–59
[8] Dai P, Nie J, Yu Y and Wu R 2024 Constraints on regional projections of mean and extreme precipitation under warming *Proc. Natl Acad. Sci.* **121** e2312400121
[9] Long S-M, Xie S-P and Liu W 2016 Uncertainty in tropical rainfall projections: atmospheric circulation effect and the ocean coupling *J. Clim.* **29** 2671–87
[10] Li C, Zwiers F, Zhang X, Li G, Sun Y and Wehner M 2021 Changes in annual extremes of daily temperature and precipitation in CMIP6 models *J. Clim.* **34** 3441–60
[11] O'Gorman P A 2012 Sensitivity of tropical precipitation extremes to climate change *Nat. Geosci.* **5** 697–700
[12] Thackeray C W, Hall A, Norris J and Chen D 2022 Constraining the increased frequency of global precipitation extremes under warming *Nat. Clim. Change* **12** 441–8
[13] Zhou W, Leung L R, Siler N and Lu J 2023 Future precipitation increase constrained by climatological pattern of cloud effect *Nat. Commun.* **14** 6363
[14] Knutti R, Meehl G A, Allen M R and Stainforth D A 2006 Constraining climate sensitivity from the seasonal cycle in surface temperature *J. Clim.* **19** 4224–33

[15] Liang Y, Gillett N P and Monahan A H 2024 Accounting for Pacific climate variability increases projected global warming *Nat. Clim. Change* **14** 608–14
[16] Hu S, Wang L, Chen X, Zhou T and Hsu P-C 2024 Emergent constraints on future projections of Tibetan Plateau warming in winter *Geophys. Res. Lett.* **51** e2024GL108728
[17] Hall A and Qu X 2006 Using the current seasonal cycle to constrain snow albedo feedback in future climate change *Geophys. Res. Lett.* **33** L03502
[18] Simpson I R, McKinnon K A, Davenport F V, Tingley M, Lehner F, Fahad A A and Chen D 2021 Emergent constraints on the large-scale atmospheric circulation and regional hydroclimate: do they still work in CMIP6 and how much can they actually constrain the future? *J. Clim.* **34** 6355–77
[19] Zhang W, Furtado K, Zhou T, Wu P and Chen X 2022 Constraining extreme precipitation projections using past precipitation variability *Nat. Commun.* **13** 6319
[20] Thackeray C W, DeAngelis A M, Hall A, Swain D L and Qu X 2018 On the connection between global hydrologic sensitivity and regional wet extremes *Geophys. Res. Lett.* **45** 11,343–51
[21] Su H *et al* 2017 Tightening of tropical ascent and high clouds key to precipitation change in a warmer climate *Nat. Commun.* **8** 15771
[22] Bretherton C S and Sobel A H 2002 A simple model of a convectively coupled Walker circulation using the weak temperature gradient approximation *J. Clim.* **15** 2907–20
[23] Fuchs Z and Raymond D J 2002 Large-scale modes of a nonrotating atmosphere with water vapor and cloud–radiation feedbacks *J. Atmos. Sci.* **59** 1669–79
[24] Fuchs Z and Raymond D J 2017 A simple model of intraseasonal oscillations *J. Adv. Model. Earth Syst.* **9** 1195–211
[25] Kim D, Ahn M-S, Kang I-S and Genio A D D 2015 Role of longwave cloud–radiation feedback in the simulation of the Madden–Julian oscillation *J. Clim.* **28** 6979–94
[26] Jakob C, Singh M S and Jungandreas L 2019 Radiative convective equilibrium and organized convection: an observational perspective *J. Geophys. Res.* **124** 5418–30
[27] Huang Y, Kim D, Zhou T and Shi X 2024 The role of cloud-radiative interaction in tropical circulation and the Madden-Julian oscillation *J. Clim.* **37** 4559–76
[28] Lin J-L and Mapes B E 2004 Radiation budget of the tropical intraseasonal oscillation *J. Atmos. Sci.* **61** 2050–62
[29] Li J-L F, Waliser D E, Stephens G and Lee S 2016 Characterizing and understanding cloud ice and radiation budget biases in global climate models and reanalysis *Meteorol. Monogr.* **56** 13.1–20
[30] Ceppi P, Brient F, Zelinka M D and Hartmann D L 2017 Cloud feedback mechanisms and their representation in global climate models *WIREs Clim. Change* **8** e465
[31] Eidhammer T, Morrison H, Mitchell D, Gettelman A and Erfani E 2017 Improvements in global climate model microphysics using a consistent representation of ice particle properties *J. Clim.* **30** 609–29
[32] John A, Douville H, Ribes A and Yiou P 2022 Quantifying CMIP6 model uncertainties in extreme precipitation projections *Weather Clim. Extremes* **36** 100435
[33] Huang Y and Shi X 2025 Codes for R–P relation paper *Zenodo* (available at: https://doi.org/10.5281/zenodo.14964799)